

# Coupling between DBI dark energy model and $f(Q)$ gravity and its effect on Condensed Body Mass accretion

Alokananda Kar<sup>1</sup>, Shouvik Sadhukhan<sup>2</sup>, and Ujjal Debnath<sup>3</sup>

<sup>1</sup>Department of Physics; Indian Institute of Technology (ISM), Dhanbad; Police Line Road, Main Campus IIT (ISM, near Rani Bandh, Hirapur, Sardar Patel Nagar, Dhanbad, Jharkhand 826004, India  
Corresponding Author Email: alokanandakar@gmail.com

<sup>2</sup>Department of Physics; Indian Institute of Space Science and Technology, Thiruvananthapuram; Valiamala Road, Valiamala, Kerala 695547  
Email: shouvikphysics1996@gmail.com

<sup>3</sup>Department of Mathematics, Indian Institute of Engineering Science and Technology, Shibpur, Howrah-711 103, West Bengal, India.  
Email: ujjaldebnath@gmail.com

## Abstract

We have studied the reconstruction formalism of the Dirac-Born-Infeld (DBI)-essence scalar field model in the background of non-metric gravity or  $f(Q)$  gravity which is controlled by the deformation or non-metricity scale  $Q$ . The deformation is caused by the fifth dimension of wrapped compact spaces in brane cosmology. The fifth dimension of that wrapped space is controlled by the D-brane tension  $T(\phi)$ . Hence, we have reconstructed the formalism of DBI scalar field energy densities and pressures using the coupling of deformation geometry and brane scalar fields, i.e.,  $f(Q)$  and DBI-Scalar fields. The accretion of dark energy onto black holes and wormholes and its critical analysis have been studied with this reconstructed model. The validity of energy conditions has been studied. We have assumed four types of singularity resolutions of the scale factor to investigate the nature of the black hole and wormhole masses due to accretion. Graphically, the physical quantities like mass, kinetic and potential energies have been analyzed for DBI-essence model in the background of  $f(Q)$  gravity.

**Keywords:** Compact body accretion, DBI-essence scalar field Dark energy,  $f(Q)$  gravity, Cosmic evolution.

## 1 Introduction

Over the years, several problems have come up while discussing the evolution of the universe, and several new theories have been put forward to explain them. The theory of inflation was introduced to explain the horizon problem, flatness problem, and magnetic monopole problem. After the discovery of the accelerated expansion of the universe, several theories were introduced

to explain this accelerated expansion since we know, of the attractive nature of gravity, accelerated expansion of gravity is not a possibility, as predicted by the Raychaudhuri equations. To explain this repulsive nature, we need the idea of negative pressure. Since no known matter can have negative pressure, the idea of dark energy (DE) was introduced, assuming that this form of energy can give the required negative pressure, which is necessary for accelerated expansion. A positive cosmological constant is the oldest form of dark energy. But this model had many shortcomings. When the experimental and theoretical data for vacuum energy differed by orders of  $10^{120}$ , scientists came up with the idea of dynamical dark energy models. Till now, several models of Dark energy have been proposed, such as the Dark fluid model (Chaplygin gas model, Tachyon model), scalar field model (DBI-essence model, Quintessence model) and holographic model. These dark energy models are efficient in providing a proper definition of negative pressure [1–5].

Modified gravity is a type of alternative gravity theory that takes higher-order terms in Einstein's action.

The theories of modified gravity are used to explain accelerated expansion. Several types of modified gravity are available in the literature. All these candidates of modified gravity have been brought depending upon the scheme of higher-order terms taken in Einstein's action.  $f(R)$  gravity, Gauss-Bonnet gravity, Teleparallel gravity and gravity with non-metricity are all included in the list of modifications of gravity. [11–21]

The modified gravity models discuss the complexities of the higher ordered Ricci tensor and scalar based action with their effect on cosmic dynamics [34]. Recent literature discusses the decompositions of these complexities using tensor decomposition calculus mechanism [1]. Teleparallel modifications are some of them [2]. In such a mechanism, the complex or higher ordered Christoffel symbol or affine connection can be decomposed to Christoffel connection for Einstein action, contortion, and the deformation of frame [35–37]. This decomposition formalism makes the geometry non-metric, and thus, we can generate the non-metric gravity or  $f(Q)$  gravity [34, 35]. Here, the term  $Q$  represents the non-metric scalar which can be written as  $Q = -\frac{1}{4}Q_{\alpha\beta\mu}Q^{\alpha\beta\mu} + \frac{1}{2}Q_{\alpha\beta\mu}Q^{\beta\mu\alpha} + \frac{1}{4}Q_{\alpha}Q^{\alpha} - \frac{1}{2}Q_{\alpha}Q^{\alpha}$  [34, 35]. The non-metric tensor can be written as  $Q_{\mu\nu} = \nabla_{\alpha}g_{\mu\nu}$ . The non-metricity is basically introduced when the Christoffel connection decomposed, and the deformation tensor is generated as the form of  $L_{\mu\nu}^{\alpha} = Q_{\mu\nu}^{\alpha} - Q_{(\mu,\nu)}^{\alpha}$  [34, 35]. Hence, the extra deformation in geometry due to the higher order modifications of Ricci tensors and metric tensors provides the non-metric counterpart of modified geometric physics [3]. When this deformation causes the negative pressure of universe expansion, this formalism can be used as an alternative to exotic energy-based cosmology or dark energy [4]. The transformation from non-decomposed geometry to decomposed geometry and the decay of deformation, as well as contortion, can provide the early time accelerated expansion or inflation of the universe [5].

Among the list of dark energy scalar field models, the DBI-essence model is the one that contains the information regarding the stringy cosmological geometry [6]. According to this model, the cosmic evolution is controlled by the D3-Brane in the warped throat region of the compact bulk space [7]. It basically modifies the invariant properties of the geometric line element, and that is why the modulation factor of Einstein Hilbert action, i.e. the  $\sqrt{-g}$  gets modifications due to the fifth-dimensional warp-factor like  $\sqrt{-det(g_{\mu\nu})} \rightarrow \sqrt{-det(A_{\mu\nu})}$  [8]. The wrap factor basically modifies the metric tensor  $g_{\mu\nu}$  [9]. This modification of metric tensor comes due to D3-Brane tension and its potential  $T(\phi)$  [10]. Using that warp factor, the modulation factor of action can be expressed as  $\sqrt{-det(A_{\mu\nu})} = \sqrt{-g}T(\phi)\sqrt{1 - \frac{\dot{\phi}^2}{T(\phi)}}$  [6, 7]. The tension potential modifies the scalar field potential of p-Brane also due to the opposing nature of  $T(\phi)$  [7, 8]. Hence, the modified potential can be written as  $V_{modified}(\phi) = V(\phi) - T(\phi)$  [8, 9]. The kinetic energy is used to modify

the modulation factor of action, and metric tensor [9, 10]. The kinetic energy of this scalar field is called non-canonical kinetic energy [6–8]. It doesn't support the canonical formalism of scalar field phase space dynamics in usual manners [7–9]. Hence, the final Lagrangian for DBI-Essence scalar fields can be written as  $\sqrt{-g}(T(\phi)\sqrt{1 - \frac{\dot{\phi}^2}{T(\phi)}} + V(\phi) - T(\phi))$  [8–10]. Thus, the transformation of such non-canonical kinetic energy into canonical kinetic energy through D3-Brane decay can provide a transformation from warp space-time to usual Einstein space-time. This can be expressed using metric tensor transformation as  $\sqrt{-det(A_{\mu\nu})} \rightarrow \sqrt{-det(g_{\mu\nu})}$ . This phenomenon can provide inflationary expansion or early time accelerated expansion of the universe. Thus, the decay of brane tension  $T(\phi)$  provides the alternative scalar field-based dark energy models or exotic type matter field-dominated universe. [6–10]

The deformation we discussed in the decomposed Christoffel Connection can be caused by the D3-Brane of warped compact bulk space-time structure. The fifth dimension type presence of D3-Brane in between the p-branes can cause the scalar field cosmic matter tension. The tension on the usual scalar field due to this fifth dimension on the warped system can provide the geometric deformation with non-metricity. Hence, both the decay of brane tension  $T(\phi)$  and the deformation factor of Christoffel connection can transfer the universe from the primordial phase to the late time phases. This transformation causes inflation. Hence, the DBI-essence model provides the dark universe through the cosmic matter scalar field point of view, whereas the  $f(Q)$  gravity provides the same through the geometric point of view. Thus, we can couple them to introduce a cause behind the deformation of geometry found from the decomposition of the Christoffel Connection. The coupled Lagrangian hence can be considered as  $L_Q + L_\phi$ . The modification of the scalar field model using the D3-brane fifth dimension is basically the modifications of matter lagrangian through scalar field energy point of view. Hence, the effective system should be coupled as  $L_Q + L_\phi + L_m$ .

The mass accretion of blackholes and wormholes mainly increases the mass of the blackholes accretion disc. In general, the compact bodies form the blackholes when their mass crosses a certain critical value beyond which it fails to exert enough hydrodynamical forces to repel the gravities due to masses. The gravitational collapse provides a boundary which splits the time outsides with the space like an inside zone. This splitting region is called the horizon. The horizons are also called null surfaces where all the killing vectors get null magnitudes, and hence, the time seems infinite w.r.t any outside observer for penetration by any arbitrary objects. Thus, the increase in mass of the black hole producing a compact body using mass accretion is impossible in physics. Hence, the accretion disc geometry evolves with such mass accretion. The accretion disc provides drag forces due to its fluid dynamics and wrapped geometry on the incoming masses. The evolution of  $f(Q)$  gravity and wrapping tension or D-brane tension evolution provides a modification on the mass accretion and its rate in the accretion disc. Hence, the drag force, fluid dynamics and the wrapping geometry in the accretion disc are indirectly modified by the evolution of modified gravity and DBI-essence scalar field dynamics. Thus, mass accretion becomes important for present universe black hole models. The wormhole geometry can be evolved with the geometry of the outside universe. The wormholes are the passage of masses through some time-like zone bounded by two throats with space-like boundaries. Hence, the evolution of the geometry of the universe and scalar fields, as well as the mass accretion, provides a modification to the throats and passage geometry. Thus, the mass accretion is linked with the geometry of blackholes and wormholes. [21, 23–26]

The primordial black holes are caused by the topological factors of the early-time inhomogeneous and anisotropic geometry. Hence, primordial black holes are called topological black holes. The topological black holes also provide horizon and deep curvatures but are caused by the early

universe phase deformations. Hence, the evolution of such deformations can also provide the evolution of the structures and equivalent masses of those topological black holes. The mass accretion in those phases is the evolution of geometries, and hence, this can modify the primordial black hole systems. [23]

The energy conditions for the universe must have to be specified due to the expansion scheme. The NEC must be satisfied, and SEC must be violated. Hence, the evolutions of the energy conditions provide the idea of the expansion scheme of the universe, which modifies the nature of black holes, as told above. Thus, energy conditions are linked with the blackholes and wormholes indirectly. [26]

In our work, we have used the local static solutions of blackholes and wormholes from Einstein's universe. We have used Schwarzschild solutions of compact bodies as blackholes and Morris-Thorne wormhole metrics in our work. The fundamental difference between the compact bodies found in modified gravity with our work is that we have used the compact bodies of Einstein's universe and modified them with mass accretion using higher order deformations. The modified gravity modifies the local solutions of blackholes and wormholes where the line elements are different from local solutions in the Einstein universe. [11–21]

The fundamental difference in mass accretion between the primordial blackholes and present-time blackholes is their nature the origin of them. The origin of present-time blackholes is the gravitational collapse, whereas the origin of primordial black holes is the topological deformations of space-time geometry due to inhomogeneous fluid and based cosmic evolutions. Hence, the mass accretion and its effects on those two blackholes are different. [11–16]

In this paper, we have concentrated on DBI-essence model of dark energy. This model takes Brane Bulk tension into account, which was not included in the previous scalar field models. Hence this is a more generalised model. Martin and Yamaguchi [6], in their work, have considered the DBI-essence field as the dark energy scalar field, where the kinetic energy term has the DBi form. Because of this, the kinetic term is non-canonical. The potential arises from the internal tension between D-branes, which controls the geometry of the warped region in compact space. Therefore, the DBI-essence model is a bit different from other slow-roll inflation models. [6–10]

In this work we have focused on  $f(Q)$  gravity which is a teleparallel modification of symmetric gravity. The metric-affine variational principle is used to obtain the symmetric teleparallel theory of gravity. The motivation for working in  $f(Q)$  gravity is that the equations of motions are in second-order, which are easier to solve. Recently in some observational analysis [7] it was found that the well-known  $f(Q)$  gravity may challenge Einstein's gravity with its viability. They have shown their analysis with Supernovae type Ia (SNIa), Baryonic Acoustic Oscillations (BAO), cosmic chronometers (CC), and Redshift Space Distortion (RSD) data that motivated us to further study on  $f(Q)$  gravity. [11–21].

Here, we have investigated the coupling between the DBI-Scalar field and  $f(Q)$  gravity. We will investigate the changes in the mass accretion rate of condensed objects caused due to these modifications. Using the Holographic technique, Babichev et al. [22] calculated the accretion of phantom DE into a Schwarzschild black hole and observed that mass decreases to zero near the big rip singularity. In this paper, we have reconstructed the DBI-essence model with modified gravity and investigated its effect on mass accretion. We have also provided the analysis of thermodynamics energy conditions to bring the acceleration in our model [23–25].

The paper is organized as follows: In sections 2 and 3, we discuss the basics of  $f(Q)$  gravity and the DBI-essence model, respectively. In section 4, we have introduced coupling between the modified gravity and dark energy model for the reconstruction mechanism. In section 5, we discuss the thermodynamic energy conditions. Section 6 contains the basic discussion on mass

accretion rate variation [27, 28]. In section 7, we take four types of scale factors [22, 25–32] and have investigated all the above-mentioned conditions. The physical analysis of the models has been discussed in section 8. Finally, we draw some conclusions from the work in section 9.

## 2 Overview of $f(Q)$ Gravity model

The action of the universe governed by  $f(Q)$  is given by [1–5]

$$S = \int \frac{1}{2} f(Q) \sqrt{-g} d^4x + \int L_m \sqrt{-g} d^4x \quad (1)$$

where  $f(Q)$  is arbitrary function of non-metricity  $Q$  and  $L_m$  is the matter Lagrangian. The non-metric tensor is defined by

$$Q_{\lambda\mu\nu} = \nabla_\lambda g_{\mu\nu} \quad (2)$$

We'll use FRW curvature free line element as

$$ds^2 = dt^2 - a^2(t)(dx^2 + dy^2 + dz^2) \quad (3)$$

The energy-momentum tensor is  $T_{\mu\nu} = (\rho_m + p_m)u_\mu u_\nu - p_m g_{\mu\nu}$  where  $\rho_m$  and  $p_m$  are respectively the energy density and pressure of matter. The effective energy momentum tensor can be written as  $(T_{\mu\nu})_{eff} = (\rho_{eff} + p_{eff})u_\mu u_\nu - p_{eff} g_{\mu\nu}$ . Here we have chosen  $8\pi G = c = 1$ . The trace of non-metric tensor with respect to line element given by (3) is

$$Q = 6H^2 \quad (4)$$

where  $H = \dot{a}/a$  is the Hubble parameter. The Friedmann equations describing the universe are

$$3H^2 = \frac{1}{2f_Q}(\rho_m - \frac{f}{2}) \quad (5)$$

and

$$2\dot{H} + 3H^2 = \frac{1}{2f_Q}(-p_m - \frac{f}{2} - 2f_Q H) \quad (6)$$

where  $\rho = \rho_m + f(Q)$  gravity energy density and  $p = p_m + f(Q)$  gravity pressure.

## 3 Overview of DBI-essence Dark Energy

DBI-essence model starts from the following action [9]

$$S = \int d^4x \sqrt{-g} (T(\phi) \sqrt{1 - \frac{\dot{\phi}^2}{T(\phi)}} + V(\phi) - T(\phi)) \quad (7)$$

The dynamical nature of scalar field can be reproduced with the Klein-Gordon equation as follows:

$$\ddot{\phi} - \frac{3T'(\phi)}{2T(\phi)} \dot{\phi}^2 + T'(\phi) + \frac{3}{\gamma^2} \frac{\dot{a}}{a} \dot{\phi} + \frac{1}{\gamma^3} (V'(\phi) - T'(\phi)) = 0 \quad (8)$$

where,  $\gamma = \sqrt{1 - \frac{\dot{\phi}^2}{T(\phi)}}$  provided  $\dot{\phi}^2 < T(\phi)$ . For simplicity, let us assume  $V(\phi) = T(\phi) = n\dot{\phi}^2$  with  $n > 1$ . So  $\gamma = \sqrt{\frac{n}{n-1}}$ .

From the modified Klein-Gordon equation, we get the kinetic energy of scalar field as follows:

$$\frac{1}{2}\dot{\phi}^2 = \frac{1}{2}\sqrt{\frac{n-1}{n}}[\rho_\phi + p_\phi] \quad (9)$$

The scalar field potential should have the form as follows:

$$V(\phi) = T(\phi) = \sqrt{n(n-1)}[\rho_\phi + p_\phi] \quad (10)$$

The scalar field component of the coupled action, we get the pressure and energy density for DBI-essence model as follows:

$$\rho_\phi = (\gamma - 1)T(\phi) + V(\phi) \quad (11)$$

And,

$$p_\phi = (1 - \frac{1}{\gamma})T(\phi) - V(\phi) \quad (12)$$

These scale factor dependent functions of density and pressure can provide us with information about DBI-essence dark energy density and pressure.

## 4 Coupling between $f(Q)$ and DBI-essence model

The reconstruction mechanism is done by introducing coupling between the reconstructing system  $f(Q)$  and the reconstructed system (DBI-essence). In our calculation, the DBI-essence scalar field is to be reconstructed. So, the coupled action can be written as follows:

$$S = \int d^4x \sqrt{-g} [\frac{f(Q)}{2} + T(\phi) \sqrt{1 - \frac{\dot{\phi}^2}{T(\phi)}} + V(\phi) - T(\phi) + L_m] \quad (13)$$

So the Friedmann equations can be written as follows:

$$3H^2 = \frac{1}{2f_Q}(\rho_m + \rho_\phi + \rho_Q) \quad (14)$$

and

$$3H^2 + 2\dot{H} = \frac{1}{2f_Q}(-p_m - p_\phi - p_Q) \quad (15)$$

From equation (5) and (6), we can write the contributions of density and pressure of  $f(Q)$  gravity for the universe as

$$\rho_Q = -\frac{f}{2} \quad (16)$$

and

$$p_Q = -f_{QQ}H\dot{Q} - \frac{f}{2} \quad (17)$$

From the scalar field components, we know that the energy density and energy density are as equations (14) and (15). Using equations (16) and (17) in (14) and (15) we get

$$\rho_\phi = 3H^2 f'(Q) - \rho_m + \frac{f}{2} \quad (18)$$

and

$$p_\phi = -(3H^2 + 2\dot{H})f'(Q) + f_{QQ}H\dot{Q} - \frac{f}{2} \quad (19)$$

where we have assumed cold dark matter with negligible pressure ( $p_m \approx 0$ ). Detailed calculation and analysis of mass accretion and other parameters will be done in the following sections.

## 5 Overview of thermodynamic energy conditions

Raychaudhuri equations in cosmic fluid dynamics provides the following energy conditions against the cosmic evolution. [33]

$$\frac{d\theta}{d\tau} = -\frac{1}{3}\theta^2 - \sigma_{\mu\nu}\sigma^{\mu\nu} + w_{\mu\nu}w^{\mu\nu} - R_{\mu\nu}u^\mu u^\nu$$

And,

$$\frac{d\theta}{d\lambda} = -\frac{1}{3}\theta^2 - \sigma_{\mu\nu}\sigma^{\mu\nu} + w_{\mu\nu}w^{\mu\nu} - R_{\mu\nu}n^\mu n^\nu$$

where  $\theta$  is the expansion factor,  $n^\mu$  is the null vector, and  $\sigma_{\mu\nu}\sigma^{\mu\nu}$  and  $w_{\mu\nu}w^{\mu\nu}$  are, respectively, the shear and rotation associated to the vector field  $u^\mu$ . Here  $\lambda$  is affine parameter. For attractive gravity we'll have the followings:

$$R_{\mu\nu}u^\mu u^\nu \geq 0 \text{ and } R_{\mu\nu}n^\mu n^\nu \geq 0$$

To set some nomenclature the energy conditions of general relativity to be considered here are

- 1 Null energy condition (NEC) or  $\rho + p \geq 0$
- 2 Weak energy condition (WEC) or  $\rho \geq 0$  and  $\rho + p \geq 0$
- 3 Strong energy condition (SEC) or  $\rho + 3p \geq 0$  and  $\rho + p \geq 0$
- 4 Dominant energy condition (DEC) or  $\rho \geq 0$  and  $-\rho \leq p \leq \rho$

## 6 Overview of Black Holes and Wormholes Mass accretion

In the case of mass accretion, the rate doesn't depend on the metric or geometry of the black holes or wormholes. Although the mass accretion of wormholes and black holes are different. We are just mentioning the basic formulae to discuss the mass accretion [27–31].

The mass accretion of black holes can be written as follows:

$$\dot{M} = -4\pi r^2 T_0^1 = -4\pi A M^2 (\rho_\phi + \rho_m + p_\phi + p_m) \quad (20)$$

The mass accretion of wormholes is given by

$$\dot{M} = 4\pi r^2 T_0^1 = 4\pi B M^2 (\rho_\phi + \rho_m + p_\phi + p_m) \quad (21)$$

We analyze the mass accretion due to the reconstructed scalar field. For further calculation, we consider cold dark matter with  $p_m = 0$ .

## 7 Different scale factor and Mass accretion

In this section, we will introduce four different scale factors as used in [25] that can produce four different results of scalar field energy densities, pressures, Scalar field kinetic energies, and scalar field potential energies. The following subsections will show all those parameters depending upon different scale factors.

Here we have used the functional form of modified gravity as follows,

$$f(Q) = \lambda Q^2 \quad (22)$$

where  $\lambda$  is a constant.

## 7.1 Scale factor $a(t) = a_0(a_1 + nt)^m$

Using the scale factor  $a(t) = a_0(a_1 + nt)^m$  in equations (20) and (21) we get,

$$\rho_\phi = -\frac{\rho_{m0}}{a_0^3(a_1 + nt)^3} + \frac{90m^4n^4\lambda}{(a_1 + nt)^4} \quad (23)$$

$$p_\phi = -\frac{48m^3n^4\lambda}{(a_1 + nt)^4} + \frac{18m^4n^4\lambda}{(a_1 + nt)^4} + \frac{12m^2n^2\lambda\left(\frac{4mn^2\lambda}{(a_1+nt)^2} - \frac{6m^2n^2\lambda}{(a_1+nt)^2}\right)}{(a_1 + nt)^2} \quad (24)$$

Here this scale factor is assumed from the idea of power-law type functions. In general, this kind of scale factor dominates the late time-expanding universe. Its range of time should be  $t > 0$  to  $t \rightarrow \infty$ . All the constants  $a_0$ ,  $a_1$ ,  $m$ ,  $n$  are positive in nature.

So, those variables can be represented graphically as follows in Figs. 1 - 4. From Fig. 1, we observe that the energy density  $\rho_\phi$  increases as time increases for  $t < 0$  (i.e., before bounce) while  $\rho_\phi$  decreases as time increases for  $t > 0$  (i.e., after the bounce) and near  $t = 0$ , the value of density is very high. On the other hand, before the bounce and after the bounce, Fig.2 shows that pressure  $p_\phi$  is very high negative near  $t = 0$ . From Figs. 3 and 4, we see that the kinetic energy and potential energy decrease from a high positive value to a low positive value as time goes on ( $t > 0$ ).

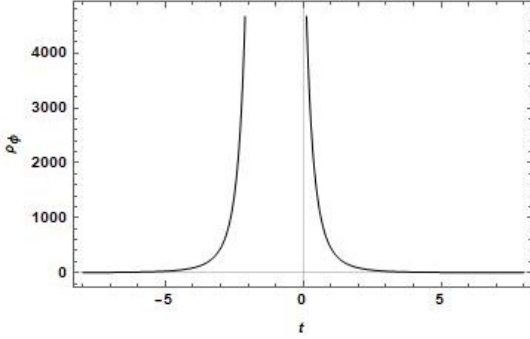


Figure 1: Plot of  $\rho_\phi$  vs  $t$  with  $a_0 = 1$ ,  $a_1 = 1$ ,  $n = 1$ ,  $\rho_{m0} = 1$ ,  $m = 2$  and  $\lambda = 5$

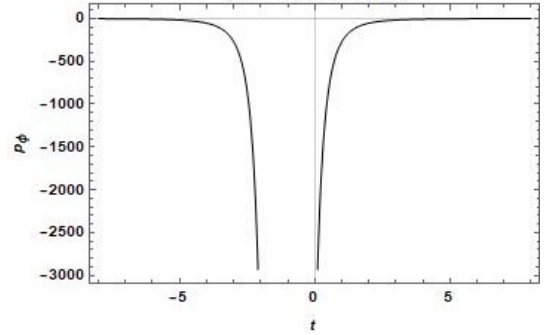


Figure 2: Plot of  $p_\phi$  vs  $t$  with  $a_0 = 1$ ,  $a_1 = 1$ ,  $n = 1$ ,  $\rho_{m0} = 1$ ,  $m = 2$  and  $\lambda = 5$

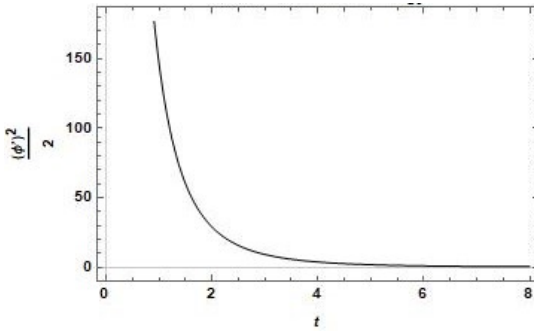


Figure 3: Plot of  $\frac{1}{2}\dot{\phi}^2$  vs  $t$  with  $a_0 = 1$ ,  $a_1 = 1$ ,  $n = 1$ ,  $\rho_{m0} = 1$ ,  $m = 2$  and  $\lambda = 5$

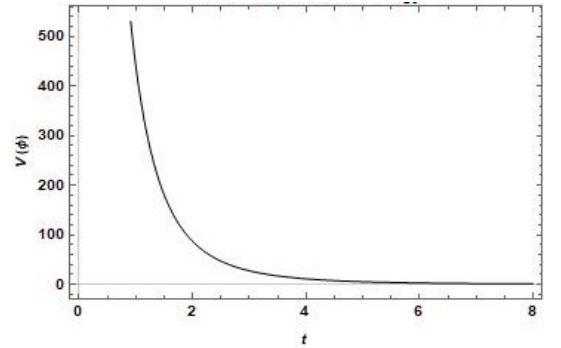


Figure 4: Plot of  $V(\phi)$  vs  $t$  with  $a_0 = 1$ ,  $a_1 = 1$ ,  $n = 1$ ,  $\rho_{m0} = 1$ ,  $m = 2$  and  $\lambda = 5$



### 7.1.1 Energy conditions with reconstructed DBI-essence model

Here we discuss the thermodynamic energy conditions. The functional form of Scalar field energy density and pressure have already been shown in the above section. Now the graphical representations for energy conditions have been shown in Figs. 5 to 7. When time increases, Figs.5,6,7 show that the SEC is violated while the NEC and DEC are satisfied.

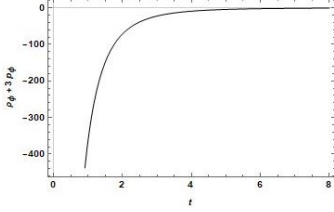


Figure 5: Plot of  $\rho_\phi + 3p_\phi$  vs  $t$  with  $a_0 = 1$ ,  $a_1 = 1$ ,  $n = 1$ ,  $\rho_{m0} = 1$ ,  $m = 2$  and  $\lambda = 5$

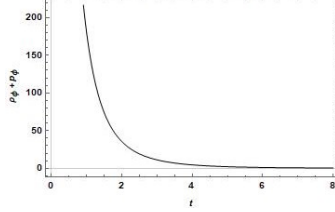


Figure 6: Plot of  $\rho_\phi + p_\phi$  vs  $t$  with  $a_0 = 1$ ,  $a_1 = 1$ ,  $n = 1$ ,  $\rho_{m0} = 1$ ,  $m = 2$  and  $\lambda = 5$

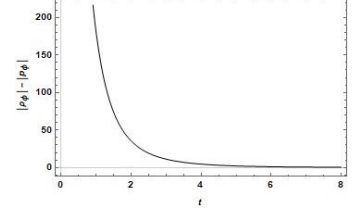


Figure 7: Plot of  $|\rho_\phi| - |p_\phi|$  vs  $t$  with  $a_0 = 1$ ,  $a_1 = 1$ ,  $n = 1$ ,  $\rho_{m0} = 1$ ,  $m = 2$  and  $\lambda = 5$

### 7.1.2 Mass accretion formalism

The basics of mass accretion have already been discussed in the above section. Now we shall discuss the mass accretion graphically for both Black holes and wormholes. The graphs have been shown as follows in figs. 8 and 9. Fig.8 shows that the mass of the black hole increases, while Fig.9 shows the decreasing nature of the wormhole mass due to the accretion of the constructed DE.

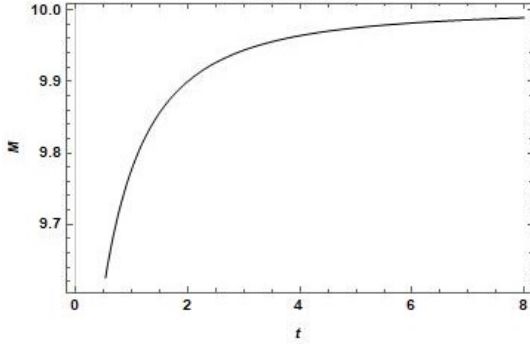


Figure 8: Plot of  $M(t)$  vs  $t$  for Black-holes with  $a_0 = 1$ ,  $a_1 = 1$ ,  $n = 1$ ,  $\rho_{m0} = 1$ ,  $m = 2$  and  $\lambda = 5$

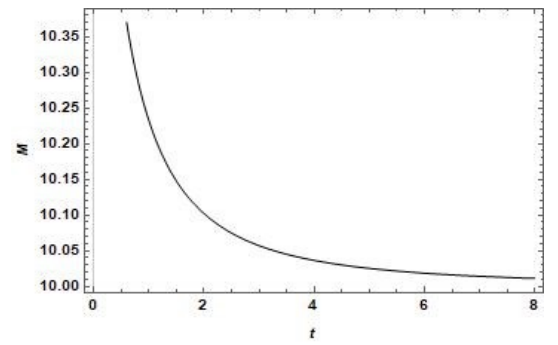


Figure 9: Plot of  $M(t)$  vs  $t$  for Worm-holes with  $a_0 = 1$ ,  $a_1 = 1$ ,  $n = 1$ ,  $\rho_{m0} = 1$ ,  $m = 2$  and  $\lambda = 5$

### 7.1.3 Reconstructed scalar field and potential

Now we'll discuss the reconstructed scalar field and its potential evolution w.r.t. the scalar field. This representation has been done with using the power law scale factor. Representations have been given in figs. 10 to 11.

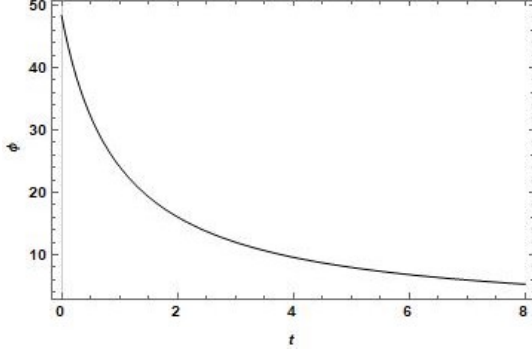


Figure 10: Plot of  $\phi$  vs  $t$   $a_0 = 1$ ,  $a_1 = 1$ ,  $n = 1$ ,  $\rho_{m0} = 1$ ,  $m = 2$  and  $\lambda = 5$

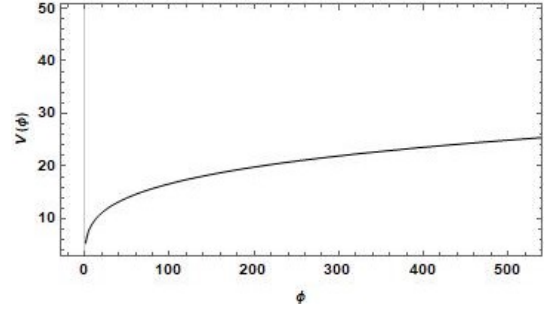


Figure 11: Plot of  $V(\phi)$  vs  $\phi$  with  $a_0 = 1$ ,  $a_1 = 1$ ,  $n = 1$ ,  $\rho_{m0} = 1$ ,  $m = 2$  and  $\lambda = 5$

## 7.2 Scale factor $a(t) = g + a_0(a_1 + nt)^m$

The scale factor  $a(t) = g + a_0(a_1 + nt)^m$  is used in equations (20) and (21) we get, the energy density  $\rho_\phi$  and pressure  $p_\phi$  which have been given in equations (27) and (28) in the **Appendix**.

This scale factor is also a special form of the first one, i.e., the power-law scale factor. This scale factor is capable of resolving the past time singularity with  $g = \text{constant}$ . We are free to choose the  $g$  as a function of time, but for simplicity, in the calculation, we have considered it as constant. For even power  $m$  the range of time should be  $t \in (-\infty, +\infty)$ .

So, those variables can be represented graphically as follows in Figs. 12-15. From Fig. 12, we observe that the energy density  $\rho_\phi$  oscillates but takes finite value as time increases from  $t < 0$  (i.e., before bounce) to  $t > 0$  (i.e., after bounce). Also, before the bounce and after the bounce, Fig. 13 shows that pressure  $p_\phi$  is oscillating with a finite negative value. We see that at  $t = 0$ , both energy density and pressure are finite, so these are regular in nature. From Figs. 14 and 15, we see that the kinetic energy and potential energy both first increase upto finite value and then decrease from a positive value to a low positive value as time goes on ( $t > 0$ ).

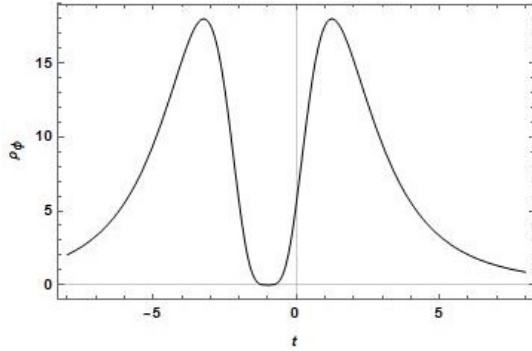


Figure 12: Plot of  $\rho_\phi$  vs  $t$  with  $a_0 = 1$ ,  $a_1 = 1$ ,  $n = 1$ ,  $\rho_{m0} = 1$ ,  $m = 2$ ,  $g = 5$  and  $\lambda = 5$

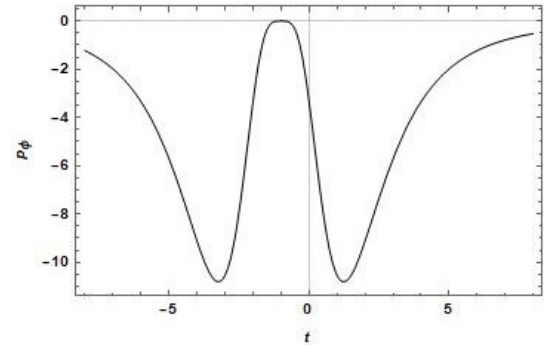


Figure 13: Plot of  $p_\phi$  vs  $t$   $a_0 = 1$ ,  $a_1 = 1$ ,  $n = 1$ ,  $\rho_{m0} = 1$ ,  $m = 2$ ,  $g = 5$  and  $\lambda = 5$

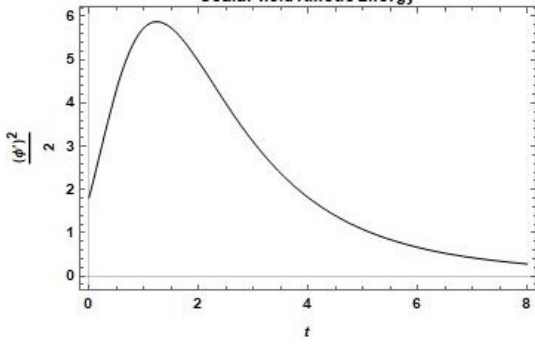


Figure 14: Plot of  $\frac{1}{2}\dot{\phi}^2$  vs  $t$  with  $a_0 = 1$ ,  $a_1 = 1$ ,  $n = 1$ ,  $\rho_{m0} = 1$ ,  $m = 2$ ,  $g = 5$  and  $\lambda = 5$

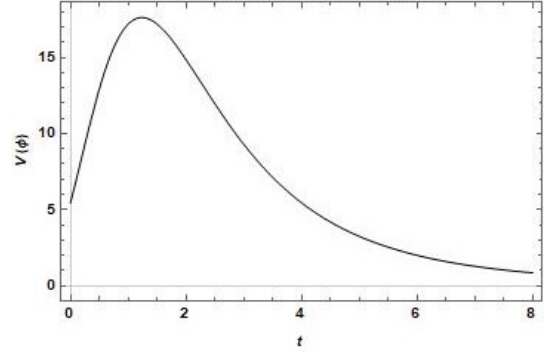


Figure 15: Plot of  $V(\phi)$  vs  $t$  with  $a_0 = 1$ ,  $a_1 = 1$ ,  $n = 1$ ,  $\rho_{m0} = 1$ ,  $m = 2$ ,  $g = 5$  and  $\lambda = 5$

### 7.2.1 Energy conditions with reconstructed DBI-essence model

We can discuss the thermodynamics energy conditions. The functional form of Scalar field energy density and pressure have already been shown in the above section. Now the graphical representations for energy conditions have been shown below in Figs. 16 to 18. When time increases, Figs. 16-18 show that the SEC is violated while the NEC and DEC are satisfied.

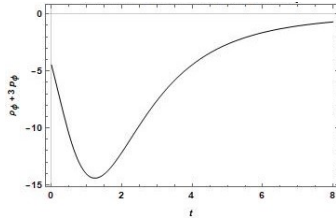


Figure 16: Plot of  $\rho_\phi + 3p_\phi$  vs  $t$  with  $a_0 = 1$ ,  $a_1 = 1$ ,  $n = 1$ ,  $\rho_{m0} = 1$ ,  $m = 2$ ,  $g = 5$  and  $\lambda = 5$

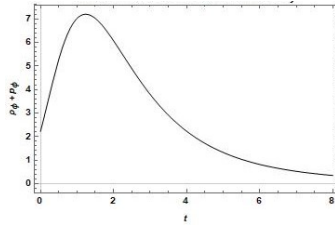


Figure 17: Plot of  $\rho_\phi + p_\phi$  vs  $t$  with  $a_0 = 1$ ,  $a_1 = 1$ ,  $n = 1$ ,  $\rho_{m0} = 1$ ,  $m = 2$ ,  $g = 5$  and  $\lambda = 5$

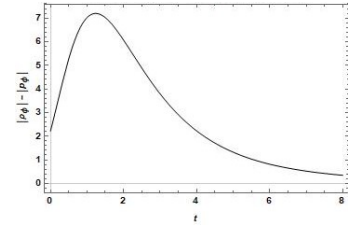


Figure 18: Plot of  $|\rho_\phi| - |p_\phi|$  vs  $t$  with  $a_0 = 1$ ,  $a_1 = 1$ ,  $n = 1$ ,  $\rho_{m0} = 1$ ,  $m = 2$ ,  $g = 5$  and  $\lambda = 5$

### 7.2.2 Mass accretion formalism

The basics of mass accretion have already been discussed in the above section. We will discuss the mass accretion graphically for both Black holes and wormholes. The graphs have been shown as follows in figs. 19 and 20. Fig.19 shows that the mass of the black hole increases, while Fig.20 shows the decreasing nature of the wormhole mass due to the accretion of the constructed DE.

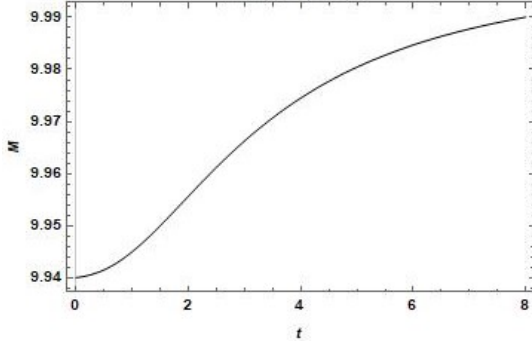


Figure 19: Plot of  $M(t)$  vs  $t$  for Black-holes with  $a_0 = 1$ ,  $a_1 = 1$ ,  $n = 1$ ,  $\rho_{m0} = 1$ ,  $m = 2$ ,  $g = 5$  and  $\lambda = 5$

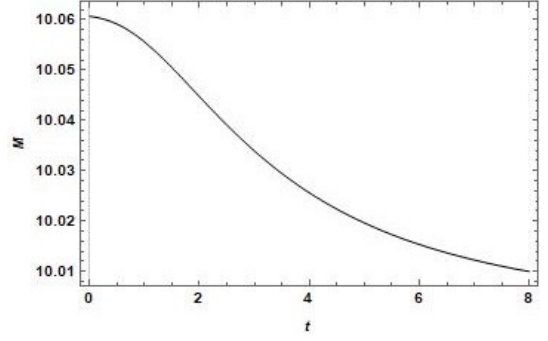


Figure 20: Plot of  $M(t)$  vs  $t$  for Worm-holes with  $a_0 = 1$ ,  $a_1 = 1$ ,  $n = 1$ ,  $\rho_{m0} = 1$ ,  $m = 2$ ,  $g = 5$  and  $\lambda = 5$

### 7.3 Scale factor $a(t) = a_0 \exp \alpha t^2$

Using scale factor  $a(t) = a_0 \exp \alpha t^2$  [25] in equations (20) and (21) we get,

$$\rho_\phi = -\frac{\rho_{m0} \exp(-3t^2\alpha)}{a_0^3} + 1440t^4\alpha^4\lambda \quad (25)$$

$$p_\phi = 384t^2\alpha^3\lambda + 288t^4\alpha^4\lambda + 48t^2\alpha^2(-8\alpha - 24t^2\alpha^2)\lambda \quad (26)$$

This scale factor has been considered to represent the inflation with the cosmic bounce together. Here also the range should be  $t \in (-\infty, +\infty)$ . So, those variables can be represented graphically as follows in Figs. 21-24.

From Fig. 21, we observe that the energy density  $\rho_\phi$  decreases and then increases from  $t < 0$  (i.e., before bounce) to  $t > 0$  (i.e., after bounce). Also, before the bounce and after the bounce, Fig. 22 shows that pressure  $p_\phi$  increases and then decreases but keeps negative value from  $t < 0$  (i.e., before bounce) to  $t > 0$  (i.e., after bounce). We see that at  $t = 0$ , both energy density and pressure are very small, so these are regular in nature. From Figs. 23 and 24, we see that the kinetic energy and potential energy both increase but keep the positive value as time goes on ( $t > 0$ ).

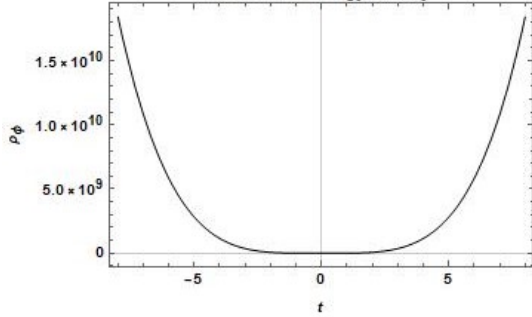


Figure 21: Plot of  $\rho_\phi$  vs  $t$  with  $a_0 = 1$ ,  $\rho_{m0} = 1$ ,  $\alpha = 5$ , and  $\lambda = 5$

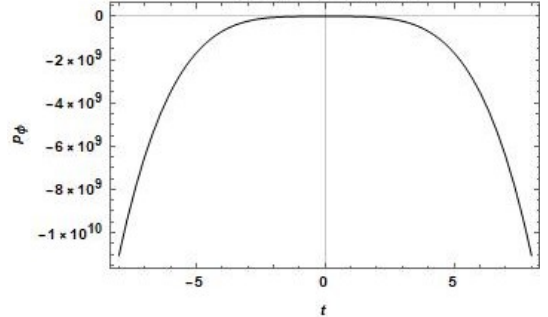


Figure 22: Plot of  $p_\phi$  vs  $t$  with  $a_0 = 1$ ,  $\rho_{m0} = 1$ ,  $\alpha = 5$ , and  $\lambda = 5$

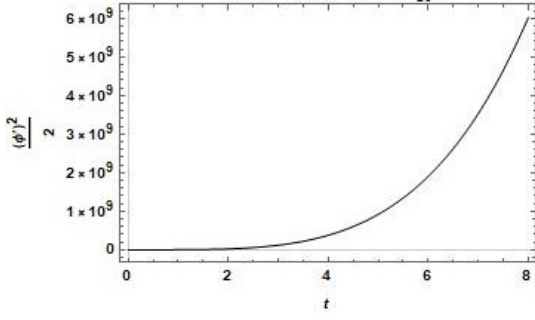


Figure 23: Plot of  $\frac{1}{2}\dot{\phi}^2$  vs  $t$  with  $a_0 = 1$ ,  $\rho_{m0} = 1$ ,  $\alpha = 5$ , and  $\lambda = 5$

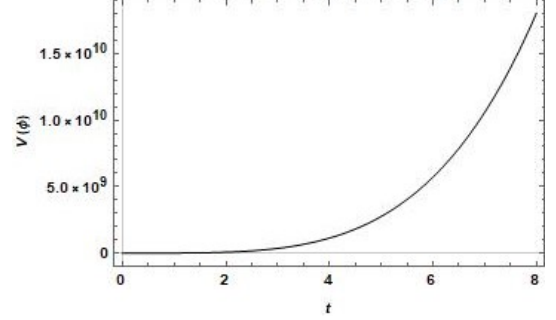


Figure 24: Plot of  $V(\phi)$  vs  $t$  with  $a_0 = 1$ ,  $\rho_{m0} = 1$ ,  $\alpha = 5$ , and  $\lambda = 5$

### 7.3.1 Energy conditions with reconstructed DBI-essence model

Here we shall discuss the thermodynamics energy conditions. The scalar field energy density and pressure found from the above calculations by assuming the 2nd type of scale factor. The functional form of Scalar field energy density and pressure have already been shown in the above section. Now the graphical representations for energy conditions have been shown in Figs. 25 to 27. When time increases, Figs. 25-27 show that the SEC is violated while the NEC and DEC are satisfied.

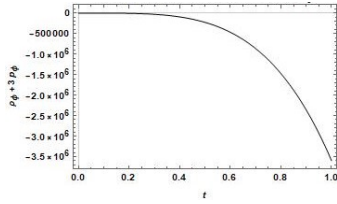


Figure 25: Plot of  $\rho_\phi + 3p_\phi$  vs  $t$  with  $a_0 = 1$ ,  $\rho_{m0} = 1$ ,  $\alpha = 5$ , and  $\lambda = 5$

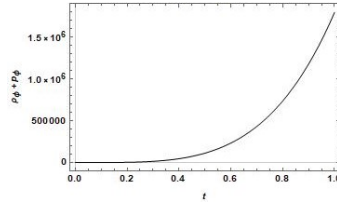


Figure 26: Plot of  $\rho_\phi + p_\phi$  vs  $t$  with  $a_0 = 1$ ,  $\rho_{m0} = 1$ ,  $\alpha = 5$ , and  $\lambda = 5$

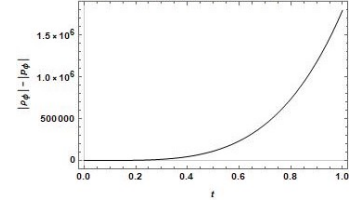


Figure 27: Plot of  $|\rho_\phi| - |p_\phi|$  vs  $t$  with  $a_0 = 1$ ,  $\rho_{m0} = 1$ ,  $\alpha = 5$ , and  $\lambda = 5$

### 7.3.2 Mass accretion formalism

The basics of mass accretion have already been discussed in section 6. Here in this section, we will discuss the mass accretion graphically for both Black holes and wormholes. The graphs have been shown as follows in Figs. 28 and 29. From these figures, we see that the masses of the black hole and wormhole decrease due to the accretion of the constructed DE.

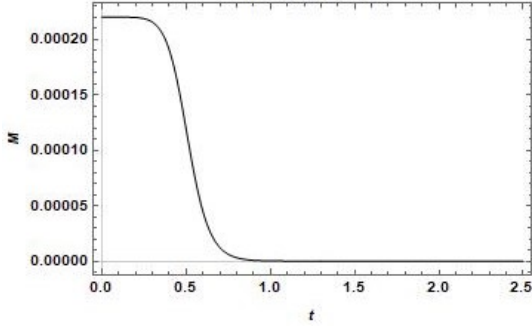


Figure 28: Plot of  $M(t)$  vs  $t$  for Black-holes with  $a_0 = 1$ ,  $\rho_{m0} = 1$ ,  $\alpha = 5$ , and  $\lambda = 5$

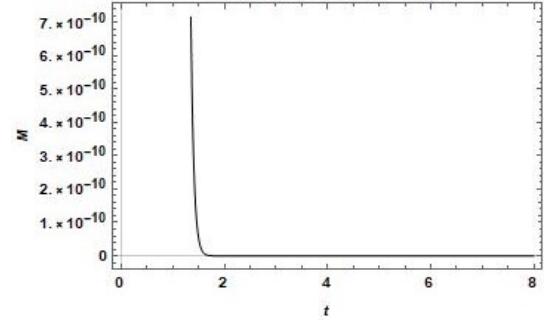


Figure 29: Plot of  $M(t)$  vs  $t$  for Worm-holes with  $a_0 = 1$ ,  $\rho_{m0} = 1$ ,  $\alpha = 5$ , and  $\lambda = 5$

#### 7.4 Scale factor $a(t) = a_0(\exp \alpha t^2 + \exp \alpha^2 t^4)$

From scale factor  $a(t) = a_0(\exp \alpha t^2 + \exp \alpha^2 t^4)$  [25] in equations (20) and (21) we get, the energy density  $\rho_\phi$  and pressure  $p_\phi$  which have been given in equations (29) and (30) in the **Appendix**.

The scale factor provides the hybrid inflationary theory with cosmic bounce. Here also the range should be  $t \in (-\infty, +\infty)$ .

So, those variables can be represented graphically as follows in Figs. 30-33. From Fig. 30, we observe that the energy density  $\rho_\phi$  decreases and then increases from  $t < 0$  (i.e., before bounce) to  $t > 0$  (i.e., after bounce). Also, before the bounce and after the bounce, Fig. 31 shows that pressure  $p_\phi$  increases and then decreases but keeps negative value from  $t < 0$  (i.e., before the bounce) to  $t > 0$  (i.e., after the bounce). We see that at  $t = 0$ , both energy density and pressure are very small, so these are regular in nature. From Figs. 32 and 33, we see that the kinetic energy and potential energy both increase but keep the positive value as time goes on ( $t > 0$ ).

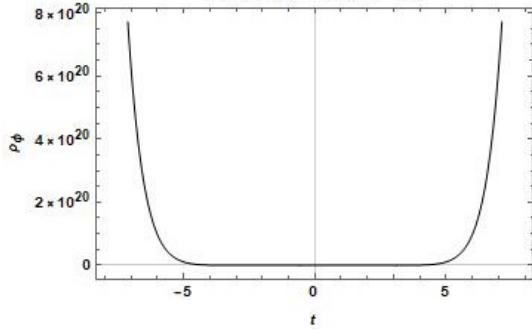


Figure 30: Plot of  $\rho_\phi$  vs  $t$  with  $a_0 = 1$ ,  $\rho_{m0} = 1$ ,  $\alpha = 5$ , and  $\lambda = 5$

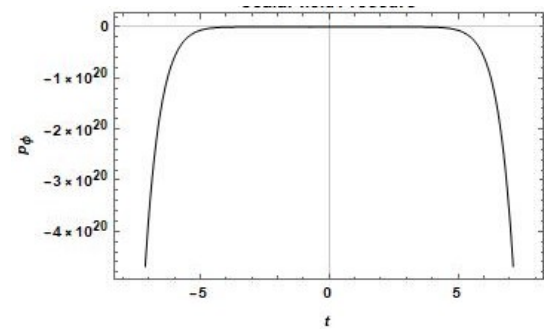


Figure 31: Plot of  $p_\phi$  vs  $t$  with  $a_0 = 1$ ,  $\rho_{m0} = 1$ ,  $\alpha = 5$ , and  $\lambda = 5$

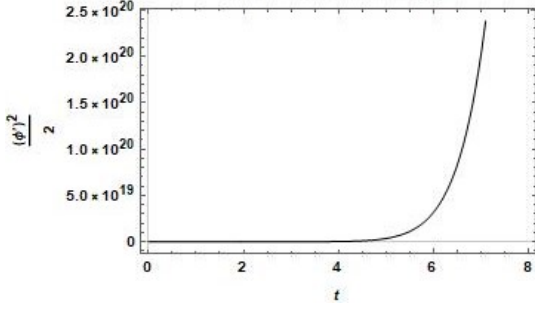


Figure 32: Plot of  $\frac{1}{2}\dot{\phi}^2$  vs  $t$  with  $a_0 = 1$ ,  $\rho_{m0} = 1$ ,  $\alpha = 5$ , and  $\lambda = 5$

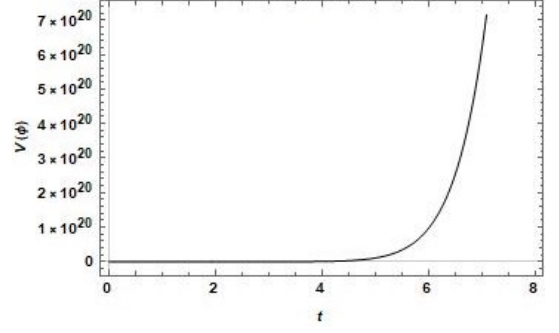


Figure 33: Plot of  $V(\phi)$  vs  $t$  with  $a_0 = 1$ ,  $\rho_{m0} = 1$ ,  $\alpha = 5$ , and  $\lambda = 5$

#### 7.4.1 Energy conditions with reconstructed DBI-essence model

The functional form of Scalar field energy density and pressure have already been shown in above section. Now the graphical representations for energy conditions have been shown in Figs. 34 to 36. When time increases, Figs. 34-36 show that the SEC is violated while the NEC and DEC are satisfied.

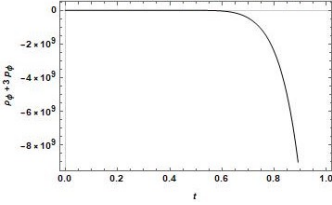


Figure 34: Plot of  $\rho_\phi + 3p_\phi$  vs  $t$  with  $a_0 = 1$ ,  $\rho_{m0} = 1$ ,  $\alpha = 5$ , and  $\lambda = 5$

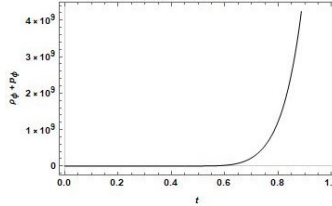


Figure 35: Plot of  $\rho_\phi + p_\phi$  vs  $t$  with  $a_0 = 1$ ,  $\rho_{m0} = 1$ ,  $\alpha = 5$ , and  $\lambda = 5$

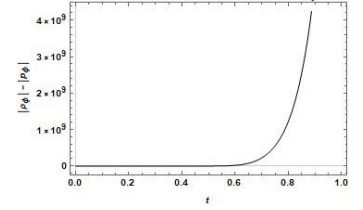


Figure 36: Plot of  $|\rho_\phi| - |p_\phi|$  vs  $t$  with  $a_0 = 1$ ,  $\rho_{m0} = 1$ ,  $\alpha = 5$ , and  $\lambda = 5$

#### 7.4.2 Mass accretion formalism

Now we will discuss the mass accretion graphically for both Black holes and wormholes, as discussed in section 6. The graphs have been shown as follows in Figs. 37 and 38. From these figures, we see that the mass of the black hole decreases while wormhole mass first slightly increases upto  $t \approx 0.3$  and then decreases due to accretion of the constructed DE.

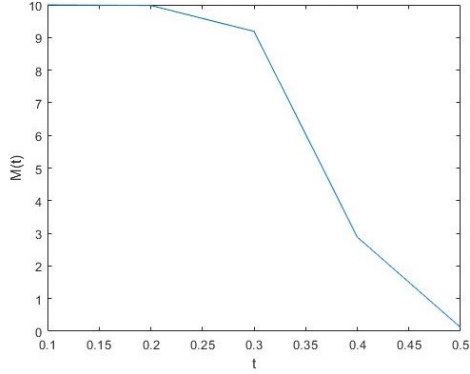


Figure 37: Plot of  $M(t)$  vs  $t$  for Black holes with  $a_0 = 1$ ,  $\rho_{m0} = 1$ ,  $\alpha = 5$ , and  $\lambda = 5$

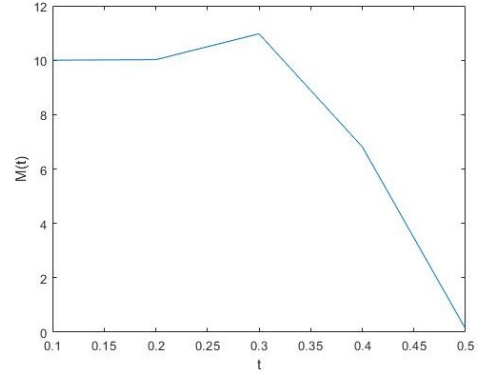


Figure 38: Plot of  $M(t)$  vs  $t$  for Wormholes with  $a_0 = 1$ ,  $\rho_{m0} = 1$ ,  $\alpha = 5$ , and  $\lambda = 5$

## 8 Physical analysis

In this work, we have considered four different types of scale factor solutions of Friedmann equations. We have analyzed energy density, pressure, scalar field kinetic energy, potential energy, thermodynamic energy conditions with density-pressure approach, and mass accretion for black holes. and wormholes with these four types of scale factors.

In figures 1, 2, 12, 13, 21, 22, 30 and 31, we have observed that all the four scale factors give positive energy density and negative pressure. These results support the observations of expanding universe. The scale factors used in this work show a concave up monotonic nature from which we can conclude that our models also support the accelerated expansion of the universe.

For the power-law type of scale factors (1st and 2nd), we have observed that the kinetic energy and potential energy both decrease with time. Particularly for the second scale factor, both energies increase at an early time and decrease at the late time (Figs. 14 and 15). But for the first type scale factor, both energies remain totally monotonic during both early and late time periods (Figs. 3 and 4). For the last two scale factors i.e., the inflationary scale factors (bouncing exponential and bouncing hybrid-exponential scale factor), we have found increasing nature of scalar field kinetic energies and potential energies (Figs. 23, 24, 32 and 33).

In the analysis of thermodynamic energy conditions (Figs. 5-7, 16-18, 25-27 and 34-36), we have observed that for the first type of scale factor, the SEC is violated, but other energy conditions are satisfied (Fig. 5 to 7). For the second type of scale factor, in the early time phase, the results for energy conditions are similar to that of the first type of scale factor. But at the late time phase, all the energy conditions are satisfied with the second type of scale factor (Fig. 16 to 18). In the last two inflationary scale factors (bouncing exponential and bouncing hybrid-exponential scale factor), we have observed that the strong energy conditions are violated, but the other energy conditions are satisfied (Figs. 25 to 27 and 34 to 36).

For the first two types of power-law scale factors, the black hole mass increases, and the rate of mass accretion also increases. On the other hand, the mass of the wormhole decreases with time. For the last two inflation-type bouncing scale factors, the masses of both black holes and wormholes decrease with time. From this, we can conclude that during late time accelerated expanding universe, the effect of gravity of black holes should be increased with time, and that of wormholes would vanish with time. The first two types of scale factors provide solutions for late time expanding model. That is why it is difficult to observe wormholes experimentally. On



the other hand, during inflations, the black holes and wormholes both should vanish, and hence it is difficult to find primordial black holes as well as wormholes experimentally at present time universe (Figs. 8, 9, 19, 20, 28, 29, 37 and 38).

For the first type of scale factor, we have represented the time evolution of scalar field and evolution of scalar field potential with respect to a scalar field. From the potential, it is observed that after a bounce, the universe should run through a slow-roll inflationary stage. The scalar field decreases continuously, and this can provide late-time warm inflation in the universe (Figs. 10 and 11).

Particularly, in the application of scale factors, we have chosen the constants and parameters (power parameter  $m$ , multiplicity parameter  $n$  and order parameter  $g$  for the first two power-law type solutions and multiplicity parameter  $\alpha$  for the last two type bouncing inflationary solutions) such that we can find a non-singular point at  $t \rightarrow 0$ . For the last two type solutions, the universe represent symmetric nature (with respect to scale factor) at  $t = 0$ . For the first two scale factors universe shows asymmetric nature in scale factor evolution.

## 9 Concluding remarks

We have discussed the reconstructed DBI-essence model with the introduction of four types of scale factors. Each scale factor represents some different cosmic phases. We have discussed the reconstructed scalar field energy density, pressure, kinetic energy, and potential energy for all those scale factors. Most of the time, we found negative pressure that provides proof of accelerated expansion of the universe.

We have discussed the energy conditions for all those scale factors. This paper compares the energy conditions and their variations for different cosmic phases.

The mass accretion also provides the idea of black holes and wormholes mass change in different cosmic phases. The first scale factor represents the late time expanding phase. The second scale factor represents the bouncing cosmic phase. The last two provide the existence of cosmic inflation by introducing the bounce.

Overall, we have tried to establish the DBI dark energy cosmology under reconstruction formalism. Although the DBI-essence is one kind of most generalized scalar field theory, our reconstructed model generalized it further which helps to represent complete evolutionary scheme of the universe.

## Appendix

Using the scale factor given in section (7.2), we get the energy density and pressure as

$$\rho_\phi = -\frac{\rho_{m0}}{(g + a_0(a_1 + nt)^m)^3} + \frac{90m^4n^4a_0^4\lambda(a_1 + nt)^{-4+4m}}{(g + a_0(a_1 + nt)^m)^4} \quad (27)$$

and

$$\begin{aligned}
p_\phi = & \left( \frac{18m^4 n^4 a_0^4 (a_1 + nt)^{-4+4m} \lambda}{(g + a_0(a_1 + nt))^m)^4} \right) \\
& + \left( \frac{4mna_0(a_1 + nt)^{-1+m} \left( -\frac{12m^3 n^3 a_0^3 (a_1 + nt)^{-3+3m}}{(g+a_0(a_1+nt))^m)^3} + \frac{6m^2 n^3 (-2+2m)a_0^2 (a_1 + nt)^{-3+2m}}{(g+a_0(a_1+nt))^m)^2} \right) \lambda}{g + a_0(a_1 + nt)^m} \right) \\
& + \left( \frac{12m^2 n^2 a_0^2 (a_1 + nt)^{-2+2m} \left( -\frac{6m^2 n^2 a_0^2 (a_1 + nt)^{-2+2m}}{(g+a_0(a_1+nt))^m)^2} - 4 \left( -\frac{m^2 n^2 a_0^2 (a_1 + nt)^{-2+2m}}{(g+a_0(a_1+nt))^m)^2} + -\frac{(-1+m)mn^2 a_0 (a_1 + nt)^{-2+m}}{(g+a_0(a_1+nt))^m} \right) \right)}{(g + a_0(a_1 + nt))^m)^2} \right)
\end{aligned} \tag{28}$$

Using the scale factor given in section (7.4), we get the energy density and pressure as

$$\rho_\phi = -\frac{\rho_{m0}}{(\exp(t^2\alpha) + \exp(t^4\alpha^2))^3 a_0^3} + \frac{90\lambda(2\exp(t^2\alpha)t\alpha + 4\exp(t^4\alpha^2)t^3\alpha^2)^4\lambda}{(\exp(t^2\alpha) + \exp(t^4\alpha^2))^4} \tag{29}$$

and

$$\begin{aligned}
p_\phi = & \left( \frac{18\lambda(2e^{\alpha t^2}t\alpha + 4e^{t^4\alpha^2}t^3\alpha^2)^4}{(e^{t^2\alpha} + e^{t^4\alpha^2})^4} \right) \\
& + \left( \frac{4(2e^{\alpha t^2}t\alpha + 4e^{t^4\alpha^2}t^3\alpha^2) \left( -\frac{12\lambda(2e^{\alpha t^2}t\alpha + 4e^{t^4\alpha^2}t^3\alpha^2)^3}{(e^{t^2\alpha} + e^{t^4\alpha^2})^3} + \frac{12(2e^{\alpha t^2}t\alpha + 4e^{t^4\alpha^2}t^3\alpha^2)(2e^{\alpha t^2}\alpha + 4e^{\alpha t^2}t^2\alpha^2 + 12e^{t^4\alpha^2}t^2\alpha^2 + 16e^{t^4\alpha^2}t^6\alpha^4)}{(e^{t^2\alpha} + e^{t^4\alpha^2})^2} \right) \lambda}{e^{t^2\alpha} + e^{t^4\alpha^2}} \right) \\
& + \left( \frac{A(B + C)}{D} \right)
\end{aligned} \tag{30}$$

where  $A$ ,  $B$ ,  $C$  and  $D$  are as follows.

$$\begin{aligned}
A &= 12\lambda(2e^{\alpha t^2}t\alpha + 4e^{t^4\alpha^2}t^3\alpha^2)^2 \\
B &= -\frac{6\lambda(2e^{\alpha t^2}t\alpha + 4e^{t^4\alpha^2}t^3\alpha^2)^2}{(e^{t^2\alpha} + e^{t^4\alpha^2})^2} \\
C &= -4 \left( -\frac{(2e^{\alpha t^2}t\alpha + 4e^{t^4\alpha^2}t^3\alpha^2)^2}{(e^{t^2\alpha} + e^{t^4\alpha^2})^2} + \frac{(2e^{\alpha t^2}\alpha + 4e^{\alpha t^2}t^2\alpha^2 + 12e^{t^4\alpha^2}t^2\alpha^2 + 16e^{t^4\alpha^2}t^6\alpha^4)}{e^{t^2\alpha} + e^{t^4\alpha^2}} \right) \\
D &= (e^{t^2\alpha} + e^{t^4\alpha^2})^2
\end{aligned}$$

## References

- [1] Solanki, R., Pacif, S.K.J., Parida, A. and Sahoo, P.K., 2021. Cosmic acceleration with bulk viscosity in modified f (Q) gravity. *Physics of the Dark Universe*, 32, p.100820.
- [2] Shekh, S.H., 2021. Models of holographic dark energy in f (Q) gravity. *Physics of the Dark Universe*, 33, p.100850.
- [3] R unkla, M. and Vilson, O., 2018. Family of scalar-non-metricity theories of gravity. *Physical Review D*, 98(8), p.084034.

- [4] Mandal, S., Wang, D. and Sahoo, P.K., 2020. Cosmography in  $f(Q)$  gravity. *Physical Review D*, 102(12), p.124029.
- [5] Frusciante, N., 2021. Signatures of  $f(Q)$  gravity in cosmology. *Physical Review D*, 103(4), p.044021.
- [6] Sen, A., 2003. Dirac-Born-Infeld action on the tachyon kink and vortex. *Physical Review D*, 68(6), p.066008.
- [7] Garousi, M.R., 2000. Tachyon couplings on non-BPS D-branes and Dirac-Born-Infeld action. *Nuclear Physics B*, 584(1-2), pp.284-299.
- [8] Sami, M., 2007. Models of dark energy. In *The Invisible Universe: Dark Matter and Dark Energy* (pp. 219-256). Springer, Berlin, Heidelberg.
- [9] Martin, J. and Yamaguchi, M., 2008. DBI-essence. *Physical Review D*, 77(12), p.123508.
- [10] Pal, S. and Chakraborty, S., 2019. Dynamical system analysis of a Dirac-Born-Infeld model: a center manifold perspective. *General Relativity and Gravitation*, 51(9), pp.1-37.
- [11] Visser, M. and Barcelo, C., 2000. Energy conditions and their cosmological implications. In *Cosmo-99* (pp. 98-112).
- [12] Chattopadhyay, S., Pasqua, A. and Khurshudyan, M., 2014. New holographic reconstruction of scalar-field dark-energy models in the framework of chameleon Brans-Dicke cosmology. *The European Physical Journal C*, 74(9), pp.1-13.
- [13] Arora, S., Santos, J.R.L. and Sahoo, P.K., 2021. Constraining  $f(Q, T)$  gravity from energy conditions. *Physics of the Dark Universe*, 31, p.100790.
- [14] Sharma, U.K. and Pradhan, A., 2018. Cosmology in modified  $f(R, T)$ -gravity theory in a variant  $\lambda(T)$  scenario-revisited. *International Journal of Geometric Methods in Modern Physics*, 15(01), p.1850014.
- [15] Sahoo, P.K., Mandal, S. and Arora, S., 2021. Energy conditions in non-minimally coupled  $f(R, T)$  gravity. *Astronomische Nachrichten*, 342(1-2), pp.89-95.
- [16] Yadav, A.K., Sahoo, P.K. and Bhardwaj, V., 2019. Bulk viscous Bianchi-I embedded cosmological model in  $f(R, T) = f_1(R) + f_2(R) f_3(T)$  gravity. *Modern Physics Letters A*, 34(19), p.1950145.
- [17] Sharma, L.K., Singh, B.K. and Yadav, A.K., 2020. Viability of Bianchi type V universe in  $f(R, T) = f_1(R) + f_2(R) f_3(T)$  gravity. *International Journal of Geometric Methods in Modern Physics*, 17(07), p.2050111.
- [18] Moraes, P.H.R.S. and Sahoo, P.K., 2017. The simplest non-minimal matter-geometry coupling in the  $f(R, T)$  cosmology. *The European Physical Journal C*, 77(7), pp.1-8.
- [19] Hulke, N., Singh, G.P., Bishi, B.K. and Singh, A., 2020. Variable Chaplygin gas cosmologies in  $f(R, T)$  gravity with particle creation. *New Astronomy*, 77, p.101357.

- [20] Singla, N., Gupta, M.K. and Yadav, A.K., 2020. Accelerating Model of a Flat Universe in  $f(R, T)$  Gravity. *Gravitation and Cosmology*, 26(2), pp.144-152.
- [21] Sharif, M., Rani, S. and Myrzakulov, R., 2013. Analysis of  $F(R, T)$  gravity models through energy conditions. *The European Physical Journal Plus*, 128(10), pp.1-11.
- [22] Babichev, E., Dokuchaev, V. and Eroshenko, Y., 2004. Black hole mass decreasing due to phantom energy accretion. *Physical Review Letters*, 93(2), p.021102.
- [23] Debnath, U., Chattopadhyay, S., Hussain, I., Jamil, M. and Myrzakulov, R., 2012. Generalized second law of thermodynamics for FRW cosmology with power-law entropy correction. *The European Physical Journal C*, 72(2), pp.1-6.
- [24] Kar, A., Sadhukhan, S. and Chattopadhyay, S., 2021. Energy conditions for inhomogeneous EOS and its thermodynamics analysis with the resolution on finite time future singularity problems. *International Journal of Geometric Methods in Modern Physics*, Vol. 18, No. 08, 2150131 (2021)
- [25] Bamba, K., Makarenko, A.N., Myagky, A.N. and Odintsov, S.D., 2014. Bouncing cosmology in modified Gauss-Bonnet gravity. *Physics Letters B*, 732, pp.349-355.
- [26] Babichev, E.O., Dokuchaev, V.I. and Eroshenko, Y.N., 2005. The accretion of dark energy onto a black hole. *Journal of Experimental and Theoretical Physics*, 100(3), pp.528-538.
- [27] Debnath, U., 2015. Accretions of dark matter and dark energy onto  $(n+ 2n + 2)$ -dimensional Schwarzschild black hole and Morris-Thorne wormhole. *Astrophysics and Space Science*, 360(2), pp.1-9.
- [28] Debnath, U., 2015. Accretion and evaporation of modified Hayward black hole. *The European Physical Journal C*, 75(3), pp.1-5.
- [29] Debnath, U., 2020. Accretion of Some Classes of Holographic DE onto Higher-Dimensional Schwarzschild Black Holes. *Gravitation and Cosmology*, 26, pp.75-81.
- [30] Jawad, A. and Shahzad, M.U., 2016. Accretion onto some well-known regular black holes. *The European Physical Journal C*, 76(3), pp.1-11.
- [31] Michel, F.C., 1972. Accretion of matter by condensed objects. *Astrophysics and Space Science*, 15(1), pp.153-160.
- [32] John, A.J., Ghosh, S.G. and Maharaj, S.D., 2013. Accretion onto a higher dimensional black hole. *Physical Review D*, 88(10), p.104005.
- [33] González-Díaz, P.F., 2006. Some notes on the big trip. *Physics Letters B*, 635(1), pp.1-6.
- [34] Jiménez, J.B., Heisenberg, L., Koivisto, T. and Pekar, S., 2020. Cosmology in  $f(Q)$  geometry. *Physical Review D*, 101(10), p.103507.
- [35] Jiménez, J.B., Heisenberg, L. and Koivisto, T., 2018. Coincident general relativity. *Physical Review D*, 98(4), p.044048.

- [36] Kar, A. and Gupta, N., 2021. Ultra-high Energy Gamma-rays from Past Explosions in our Galaxy. arXiv preprint arXiv:2112.08757.
- [37] Anagnostopoulos, F.K., Basilakos, S. and Saridakis, E.N., 2021. First evidence that non-metricity  $f(Q)$  gravity could challenge  $\Lambda$ CDM. Physics Letters B, 822, p.136634.